IEEE Access
Multidisciplinary ⋮ Rapid Review ⋮ Open Access Journal

Received May 22, 2021, accepted June 3, 2021, date of publication June 8, 2021, date of current version June 18, 2021.

Digital Object Identifier 10.1109/ACCESS.2021.3087613

Optimal Design of Hemispherical 7-Hole Probe Tip With Perpendicular Holes

TAO YAO[1], SHU-DAO ZHOU[1], MIN WANG[2], SONG YE[1], AND YANG-CHUN ZHANG[1]
[1]College of Meteorology and Oceanography, National University of Defense Technology, Nanjing 211101, China
[2]School of Electronic and Information Engineering, Nanjing University of Information Science and Technology, Nanjing 210044, China

Corresponding author: Min Wang (yu0801@163.com)

This work was supported by the National Natural Science Foundation of China under Grant 41775039 and Grant 41775165.

ABSTRACT The 7-hole probe measurement system is mainly used to measure three-dimensional flow fields. During the measurement, the probe head was in direct contact with the measured object, and the head structure had a significant influence on the accuracy of the flow field measurement. The main influencing factors were the hole opening mode, hole position, and hole diameter. For a hemispherical 7-hole probe with perpendicular and forward-facing holes, orthogonal experiments with three levels and three factors (inflow velocity, hole position, and hole diameter) were designed, and additional experiments were conducted on the significant factors. The importance of factors was evaluated based on the correlation between different structural parameters and the pressure coefficient. The experiment was simulated using FLUENT, and the numerical simulation results demonstrated that the square of deviance at the inlet velocity, hole diameter, and hole position was 0.0018, 0.0013, and 0.3611, respectively. The position of the hole has a significant influence on the measurement results, but the influence of the inflow velocity and hole diameter is negligible, and the pressure coefficient is the smallest when the hole is at 45°. For the hemispherical 7-hole probe with forward facing hole, the hole is the best at approximately 45°, and considering the convenience of processing, the diameter of the hole can be selected as the diameter of the 1/10 probe.

INDEX TERMS 7-hole probe, perpendicular hole, structure optimization, numerical simulation.

I. INTRODUCTION

Multi-hole probes are often used to measure three-dimensional (3D) flow fields. With proper calibration, this information can then return three components of the fluid velocity, as well as static and dynamic pressures [1]–[4]. In addition to the multi-hole probe, hot wire anemometer (HWA), and laser doppler velocimetry (LDV), particle image velocimetry (PIV) systems are widely used in the detection of 3D flow fields. However, the HWA sensor is relatively fragile and unsuitable for measuring highly dynamic and complex fluids [5]. Meanwhile, the LDV response time is too long to adequately reflect the flow field information in real time, and the PIV tracer itself causes disturbances in the flow field and introduces unnecessary errors. Because of its simple structure and strong adaptability to the environment, the multi-hole probe is widely preferred in the measurement of various complex flow fields. There are different shapes of multi-hole probes: the number of holes is generally odd, with 5,7, and 17 holes,from the tip shape, there are spherical, hemispherical, conical, and pyramid shapes. For the hole opening mode, there are forward facing (the hole axis parallel to the probe axis) and perpendicular holes (vertical probe surface) [6]–[8]. The maximum angle that can be detected by a 5-hole probe is limited to 55°, whereas the measuring angle of a 7-hole probe can reach 75° [9]. Therefore, the 5-hole probe is often used in turbomachinery and in other scenarios. When the probe needs to be used in the aerospace field, a 7-hole probe that can measure a wider angle range is required. The measurement range of the 17-hole probe is as high as 150° and can be used for almost omni-directional measurements [7]; however, it is very expensive and useful only in a few cases where rear inflow measurement is needed. Theoretically, any tip shape would work for a multi-hole probe. James Crawford [10] studied the correlation between the shape of the 7-hole probe tip and the sensitivity of the Reynolds number, and highlighted that the hemispherical tip is less dependent on the Reynolds number. Therefore, this study focuses on a hemispherical 7-hole probe.

The associate editor coordinating the review of this manuscript and approving it for publication was Huaqing Li.

When a 3D flow field is detected by a multi-hole probe, the fluid flows near the probe surface. If there is a hole on the probe surface, it will inevitably affect the flow field near the probe, causing an error between the actual measured pressure and the probe surface pressure. If the hole is larger on the surface of the probe, the error is greater. To facilitate machining, the existing 7-hole probes combine seven thin tubes together through welding [11]; therefore, almost all of them are forward-facing holes. When the probe measures the flow field, in most cases, the probe hole has a positive convective flow, and the flow in a deeper part of the hole is still turbulent. The hemispherical 7-hole probe with perpendicular holes is a vertical probe surface [12], and the field near the probe hole will not flow directly into the probe hole, which also meets the requirements of static pressure measurement. At present, only the shape optimization of the probe tip has been studied [10], [13], and the position of the hole has not been discussed. In this study, we investigated the determination of the optimal opening method of the probe to make the measured pressure closer to the real pressure on the probe surface. To study the optimal structure of the tip with a hemispherical 7-hole probe, FLUENT software was used for the numerical calculation of the perpendicular and forward-facing holes under the hole diameter, hole position, and flow velocity. The optimal structure of the tip with a hemispherical 7-hole probe was determined by analyzing the pressure coefficient of the probe hole.

II. PROBE STRUCTURE PARAMETERS AND TEST DESIGN

A. STRUCTURAL PARAMETERS OF THE HEMISPHERICAL 7-HOLE PROBE

When measuring the 3D flow field, the probe was completely immersed in the flow field. If the probe surface has a hole, the flow field will be affected to varying degrees [14], [15], which causes the measured pore pressure to deviate from the spherical static pressure. The aperture size, hole position, and hole opening mode are all factors that affect the measurement accuracy of the probe. Taking a hemispherical probe with a diameter of 6 mm as an example, its structure is shown in Fig. 1. By analyzing the influence of hole diameter D, hole angle (hole position L), and hole opening mode on pressure measurement at different inflow velocities, the optimal hole opening scheme is comprehensively selected. Considering the machining problem, the range of hole diameter is 0.4-0.8 mm, whereas that for the hole angle is 30–60°, and the application scene is a subsonic flow field; therefore, the velocity range is 10-100 m/s.

B. TEST PROGRAM

There are three structural factors to be considered for the perpendicular and forward-facing hole probes: hole diameter D, hole angle (hole position L), and flow field velocity. If each factor takes three levels, $3^3 = 27$ experiments will be conducted, which will require a significant amount of time and computational resources. The experimental optimization design has good orthogonality and uniformity, and it reflects the comprehensive test well under the condition of a reduction in the number of experiments. Therefore, the orthogonal test is a very effective experimental method used to conduct multiple factor experiments to shorten the cycle of the experiment [16]. For the three values of the significant factors, the optimal value cannot be obtained simultaneously, and approximate additional experiments should be conducted according to the preliminary test results. According to the design method of the orthogonal table, an experiment with three factors and three levels were designed, as summarized in Table 1 and 2.

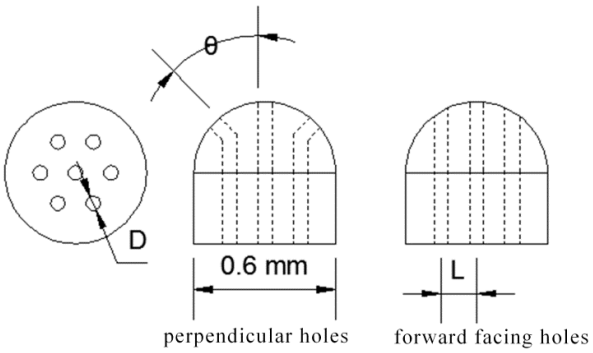

FIGURE 1. 7-hole probe structure diagram.

TABLE 1. Orthogonal test of perpendicular holes.

Level serial	Factors		
	v(m/s)	θ (°)	D(mm)
1	10	30	0.4
2	50	45	0.6
3	100	60	0.8

TABLE 2. Orthogonal test of forward-facing holes.

Level serial	Factors		
	v(m/s)	L(mm)	D(mm)
1	10	1.5	0.4
2	50	2.12	0.6
3	100	2.6	0.8

III. NUMERICAL SIMULATION

The number of probe experiments is reduced to nine in an orthogonal experimental design. If a probe with perpendicular and forward-facing holes is performed in a wind tunnel test, nine probes with different structures are required and the cost is high, and with the development of computational fluid dynamics, through computer numerical calculation, the numerical solution of the flow field is described quantitatively in time and space [17], which saves time and reduces research costs.

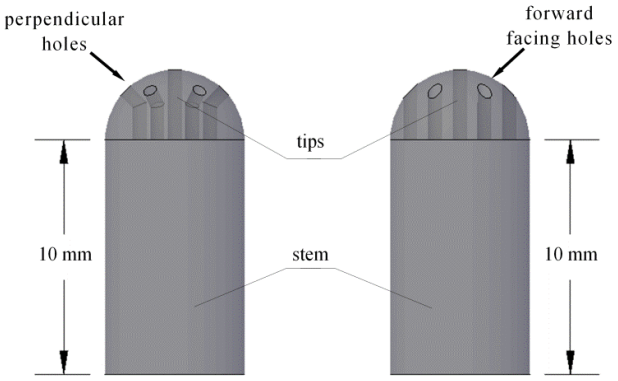

FIGURE 2. 3D model of probe.

A. TURBULENCE MODEL

Turbulent flow is a common flow phenomenon in nature. In most engineering problems, the flow of fluid is often in a turbulent state. At present, numerical simulation of turbulence can be divided into direct numerical simulation (DNS), large eddy simulation (LES), and Reynolds average method (RANS). Both DNS and LES involve a relatively significant amount of calculation. RANS is used to derive several turbulence models based on different simplifications of turbulence; among them, the Spalart–Allmaras single-equation model is specially used to solve the wall-restricted flow in the aviation field, and it has a remarkable effect on the boundary layer flow under the action of the inverse pressure gradient. The governing equations are as follows:

$$\frac{\partial}{\partial t}(\rho\tilde{v}) + \frac{\partial}{\partial x_i}(\rho\tilde{v}u_i) = G_v + \frac{1}{\sigma_{\tilde{v}}}\left[\frac{\partial}{\partial x_j}\left\{(\mu + \rho\tilde{v})\frac{\partial\tilde{v}}{\partial x_j}\right\} + C_{b2\rho}\left(\frac{\partial\tilde{v}}{\partial x_j}\right)\right] - Y_v + S_{\tilde{v}} \quad (1)$$

where $\tilde{v}$ is the turbulent viscosity except for the near-wall area, G_v is the turbulent viscosity term, Y_v is the failure viscosity term of the closed wall and viscous damping near the wall, $\sigma_{\tilde{v}}$ and $C_{b2\rho}$ is a constant, v is the molecular dynamic viscosity, and $S_{\tilde{v}}$ is a user-defined source item.

B. GEOMETRIC MODELING AND MESHING

The tips of the hemispherical 7-hole probe consisted of one center hole and six static pressure holes, and six static pressure holes were distributed near the center hole. Considering that the two-dimensional model of the symmetrical section only reflects the flow of this section, whereas the mapping to the 3D space reflects the flow near the cylinder, a 3D hemispherical 7-hole probe model is constructed. To simulate the real conditions as much as possible and prevent backflow from interfering with the flow field of the tip, a probe stem of 10 mm was added at the back of the tip. The hemispherical 7-hole probe model with perpendicular and forward-facing holes is shown in Fig. 2.

TABLE 3. Different grid number.

Situation	1	2	3	4
Grid number	291000	449812	934338	1477284

TABLE 4. Calculation results of different grids.

Grid Situation	Pressure of the center hole/Pa	Variance of pressure/Pa	Probe surface pressure/Pa
1	6642	1126.32	3224
2	6642	2029.67	3225.5
3	6638	146.04	3205.5
4	6637	272.16	3204.25

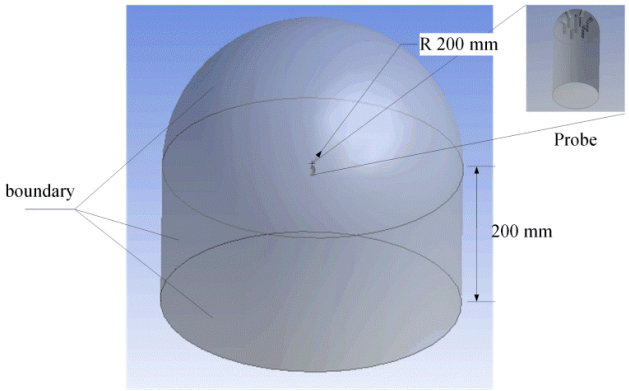

FIGURE 3. Probe calculation domain.

A space composed of a radius of 200 mm hemisphere and a height of 200 mm cylinder was established outside the probe, and the probe geometry model was excavated inside the space as the computational domain of the fluid simulation, as shown in Fig. 3.

The meshing method adopts the hexahedral-based cutcell method to mesh the computational domain. To determine that there is no correlation between the number of grids required for calculation and the technical results, it is necessary to test the grid independence. The parameter of significant interest in this simulation is the surface pressure of the probe. Point a on the probe surface, the pressure of the center hole, and the variance of pressure of the outer six holes are selected to check the grid independence. Then, the four grid numbers shown in Table 3 are calculated. The calculation results are shown in Table 4 and figure 3. The calculation results are shown in Table 4.

It can be seen that the number of grids has increased from 934338 to 1477284, and the pressure values of the three positions have only changed slightly. This suggests that increasing the number of grids beyond 934338 has little effect on the calculation results; hence, it suffices to choose 934338 as the number of grids. Fig. 4 shows the grid partition of the computational domain and the grid partition of the probe hole.

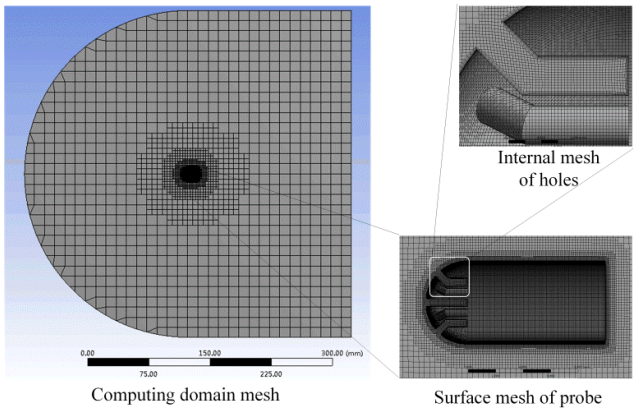

FIGURE 4. Grid division of flow field.

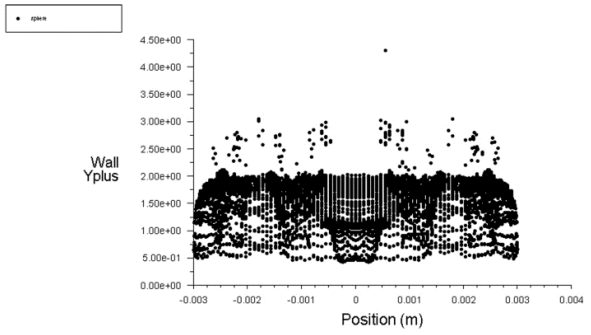

FIGURE 5. y^+ value of probe surface.

In order to verify the rationality of the boundary layer grid, the calculated y^+ value is checked. Figure 5 shows the distribution of y^+ value on the surface of the probe, which can be seen that it is basically distributed between 0.5 and 2, so the meshing of the boundary layer can meet the calculation requirements.

C. FLOW FIELD CONDITION SETTING

The multi-hole probe is applied to the middle atmosphere environment, with ideal air chosen as the domain medium for the calculation. The calculation is performed at a temperature of 273 K, and the dynamic viscosity of air at 273 K is $1.716 \times 10^{-5} Pa \cdot s$. The atmospheric pressure at the bottom of the stratosphere is 1/3 that of the sea level atmospheric pressure; thus, a pressure of 33775 Pa is selected as the absolute pressure for numerical calculation. The air density in dry air is only related to the absolute pressure and temperature, which can be obtained as follows:

$$\rho = \rho_0 \frac{273}{273+t} \times \frac{p}{0.1013} \tag{2}$$

where ρ is the density of dry air at temperature t and pressure p, ρ_0 is the density of dry air at a temperature of 0 °C and a pressure of 0.1013 MPa, equal to 1.293 kg/m^3, p is the absolute pressure, and (273+t) is the thermodynamic temperature. The density of air at a temperature of 273 K and pressure of 33775 Pa was computed to be 0.431 kg/m^3. The initial conditions of the flow field are as shown in Table 5.

TABLE 5. Flow field condition.

Parameter	Value
Temperature / K	273
dynamic viscosity / $Pa \cdot s$	1.716×10^{-5}
Absolute pressure / Pa	33775
Density / kg / m^3	0.431

After determining the flow field conditions, the Reynolds number on the surface of the probe and inside the hole can be calculated as follows:

$$\mathrm{Re} = \frac{\rho u L}{\mu} \tag{3}$$

where ρ is the fluid density, u is the flow rate, L is the characteristic length, and μ is the dynamic viscosity. When the speed range is 10–100 m/s, the range of the Reynolds number of the flow on the probe surface is 1500–15000 and the range of Reynolds number of the flow in the hole is 100–2000.

IV. INFLUENCE OF PROBE STRUCTURE PARAMETERS

The evaluation of the influence of different structural parameters on the probe measurement is essentially to evaluate the accuracy of pressure measurement by seven pressure holes. Pressure coefficient C_p is usually used to evaluate static pressure measurement by pressure hole. The smaller the absolute value of pressure coefficient C_p is, the better the accuracy of static pressure measurement is [18]. The calculation formula of C_p is

$$C_p = \frac{P_i - P_\infty}{1/2 \rho U_\infty^2} \tag{4}$$

where P_i is the pressure measured by the pressure hole, P_∞ is the static pressure of the flow field, ρ is the gas density of the flow field, and U_∞ is the inflow velocity.

A. INFLUENCE OF HOLE POSITION

Ignoring the influence of the hole on the surface pressure of the probe, a curve without hole in the sphere is selected to represent the distribution of the pressure coefficient of the sphere at different positions, and the variation curve of the pressure coefficient on the sphere with the position L is shown in figure 6. Compared with the simulation results for the unperforated sphere, the minimum pressure coefficient is 70.5° [19]. Because this simulation involves a sphere with holes, with the angle of the minimum pressure coefficient point d being 76°, the simulation results can be considered reliable. It can be seen that the pressure coefficient at different positions on the surface of the probe is different. The pressure coefficient becomes smaller with the distance away from the center hole, the pressure coefficient becomes zero near point a, and the absolute value of the pressure coefficient increases

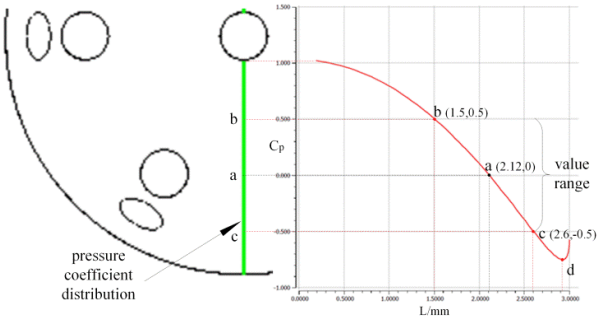

FIGURE 6. Variation curve of pressure coefficient of probe surface with hole position.

gradually with the increase of the distance. It can be seen from Fig. 6 that when the pressure coefficient is lower than −0.5, a pressure coefficient value corresponds to two spherical positions, which is absolutely not allowed in measurement. The pressure coefficient should be controlled in the range of −0.5–0.5, the corresponding angle range of perpendicular holes is 30–60°, and distance L of forward-facing holes is 1.5–2.6 mm.

B. INFLUENCE OF HOLE DIAMETER

The probe pressure hole is a channel to transfer pressure, and a pressure sensor is installed at the back of the hole to detect pressure. Too small hole diameter will increase the hysteresis error and improve the risk of hole blockage. Too large hole diameter will affect the accuracy of measurement. Fig. 7 shows the velocity contours of the probe section under different pore diameters of the probe with perpendicular holes and forward-facing holes, respectively.

It can be seen from the diagram that whether it is perpendicular holes or forward-facing holes, the flow in the front of the hole is unsteady. With the increase of the hole diameter, the gas disturbance inside the hole increases gradually, and gradually develops to the depth of the hole. It can be seen that the larger the hole diameter, the more unstable the flow inside the hole, which will affect the accuracy of the measured hole pressure.

C. INFLUENCE OF HOLE MODE

If the hemispherical seven-hole probe is to weld seven long pipes with small inner diameter together, the probe with forward-facing holes is processed. When the probe is facing the incoming flow, the flow field inside the hole is unstable for a long distance. When the position of the hole is far away from the center hole, the area of the hole formed on the sphere will be much larger than perpendicular holes. By comparing the velocity contours of perpendicular holes and forward-facing holes under different diameter in Fig. 7, it can be seen that the flow field of the forward-facing hole probe is still unstable in the deeper part of the hole. The perpendicular hole probe tends to be almost stable after the corner, and the stable convergence of the forward-facing hole is worse than that of the perpendicular hole when the diameter increases.

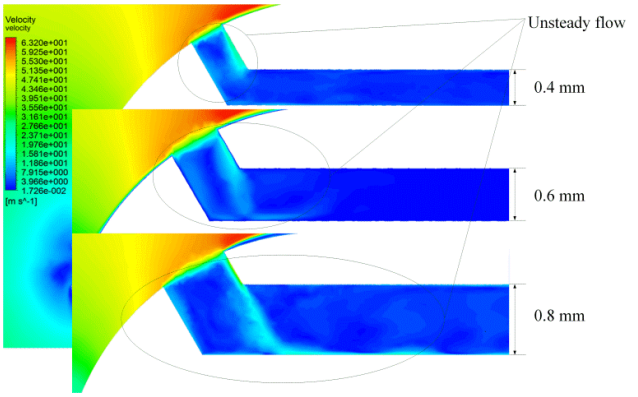

(a) perpendicular holes

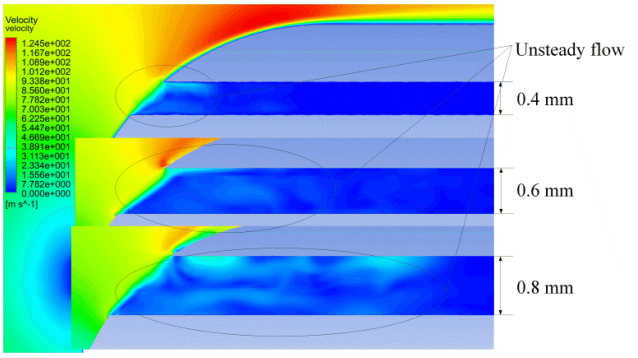

(b) forward faceing holes

FIGURE 7. Velocity contours of probes with different apertures.

Under the same flow field conditions, nine groups of experimental designs of the perpendicular hole probe and the forward-facing hole probe were simulated, and the pressure coefficient results are shown in Table 6. Among them, C_{P1} is the average pressure coefficient of the six static pressure holes of the perpendicular hole probe, and C_{P2} is the average pressure coefficient of the six static pressure holes of the forward-facing hole probe. It can be seen from Table 6 that, except for some values, the value of C_{P2} is greater than that of C_{P1} in general, indicating that the perpendicular hole has little influence on the probe measurement result compared with the forward-facing hole.

V. RESULT ANALYSIS

In order to obtain the influence of different structural parameters of the probe on the pressure coefficient, it is necessary to further variance analysis and range analysis of the pressure coefficient C_{P1} of the perpendicular hole probe. The results are shown in table 7.

In Table 7, $\bar{y}_{jk}$ represents the average value of the static pressure coefficient corresponding to the k level of factor j, and the optimal level of factor j can be judged by the value of $\bar{y}_{jk}$. R_j is the extreme difference, and S_j is the square of deviance. f_j is the degree of freedom, and F_j is the F distribution.

TABLE 6. Simulation results of pressure coefficient.

Test number	Factor			Index	
	v (m/s)	θ (°)	D (mm)	C_{P1}	C_{P2}
1	10	30	0.4	0.5375	0.5654
2	10	45	0.6	0.0801	0.2079
3	10	60	0.8	0.3763	0.2280
4	50	30	0.6	0.5551	0.5895
5	50	45	0.8	0.1146	0.1831
6	50	60	0.4	0. 4270	0.2203
7	100	30	0.8	0.6087	0.6399
8	100	45	0.4	0.0564	0.1540
9	100	60	0.6	0.3907	0.2899

TABLE 7. Pressure coefficient C_{P1} analysis.

Serial factor	1	2	3
	v (m/s)	θ (°)	D (mm)
$\bar{y}_{j1}$	0.3313	0.5671	0.3403
$\bar{y}_{j2}$	0.3656	0.0837	0.3420
$\bar{y}_{j3}$	0.3519	0.3980	0.3665
R_j	0.0343	0.4834	0.0262
S_j	0.0018	0.3611	0.0013
f_j	2	2	2
F_j	0.65	131.36	0.47

A. EXTREMUM DIFFERENCE ANALYSIS

Extremum difference R_j reflects the variation range of the test index when the level of factor j changes [16]. The larger R_j is, the greater the effect of this factor on the test index is, so it is more important. The primary and secondary factors in the experiment can be determined by the magnitude of extremum difference R_j. The calculation formula is

$$R_j = \max\left[\bar{y}_{j1}, \bar{y}_{j2}, \bar{y}_{j3}\right] - \min\left[\bar{y}_{j1}, \bar{y}_{j2}, \bar{y}_{j3}\right] \tag{5}$$

The S_j is the square of deviance of the average and the total average of the test index corresponding to the level of factor j [16], indicating the fluctuation of the test data caused by the level change of this factor. The calculation formula is

$$S_j = \frac{a}{b}\sum_{k=1}^{b}\left(\bar{y}_{jk} - \bar{y}\right)^2 \tag{6}$$

where a is the total number of tests, b is the number of horizontal occurrences of the column, and $\bar{y}$ is the average value of test index C_{p1}.

It can be seen from Table 6 that $R_2 = 0.4834 \gg R_1 = 0.0343 > R_3 = 0.0262$, the extremum difference of pressure coefficient of hole angle is much larger than that of velocity and hole diameter, the influence of hole angle on pressure coefficient is much larger than that of velocity and hole diameter. It can be obtained that the hole angle is the main factor affecting the pressure coefficient of the probe, and the hole diameter and flow velocity are the secondary factors; $S_2 = 0.3611 \gg S_1 = 0.0018 > S_3 = 0.0013$, the deviation square sum of the pressure coefficient of the hole angle is much larger than that of the velocity and the diameter of the hole. The change of the hole angle has a great influence on the pressure coefficient, and the change of the velocity and the diameter of the hole has little influence on the pressure coefficient.

TABLE 8. Additional experiment results.

Test number	Factors			Index
	v (m/s)	θ (°)	D (mm)	C_{P1}
10	10	40	0.4	0.2237
11	10	50	0.8	0.0748
12	50	40	0.6	0.2356
13	50	50	0.4	0.1263
14	100	40	0.8	0.3307
15	100	50	0.6	0.0832
$\bar{y}_{j1}'$	0.2288	0.5671	0.2379	
$\bar{y}_{j2}'$	0.2536	0.0837	0.2375	
$\bar{y}_{j3}'$	0.2544	0.3980	0.2700	
$\bar{y}_{j4}$	—	0.2633	—	
$\bar{y}_{j5}$	—	0.0948	—	

B. SIGNIFICANCE TEST

After variance analysis, it is necessary do the significance test to determine its confidence level. In Table 7, F_j is a random variable of F distribution with degree of freedom of (f_j, f_e), and its calculation formula is

$$F_j = \frac{S_j/f_j}{S_e/f_e} \tag{7}$$

where $S_e = 0.0027$ is the error of square of deviance, $f_e = 2$ is the freedom level of error. Select significance $\alpha = 0.01$, from the F distribution table $F_{0.01}(2, 2) = 99.01 < F_2 = 131.36$, it can be considered that the hole angle has a significant effect on the pressure coefficient and its confidence level is 99%. The values of F_1 and F_3 are less than 1, which can be considered that the velocity and hole diameter have little effect on the pressure coefficient.

C. ADDITIONAL TEST

Through variance analysis and significance test, it can be seen that the hole angle has a significant effect on the pressure coefficient. The optimal level cannot be found only through

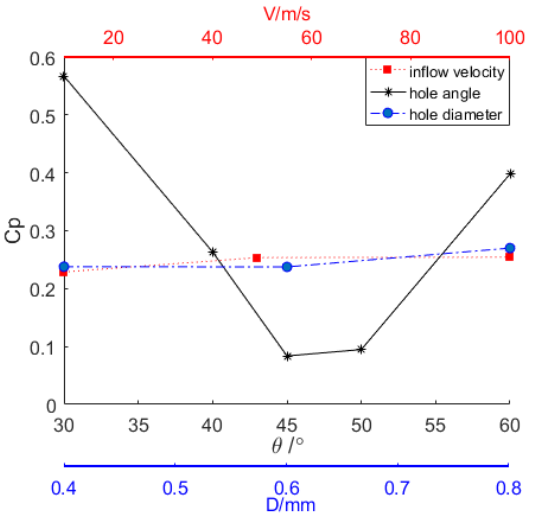

FIGURE 8. Influence of pressure coefficient changes with the level of each factor.

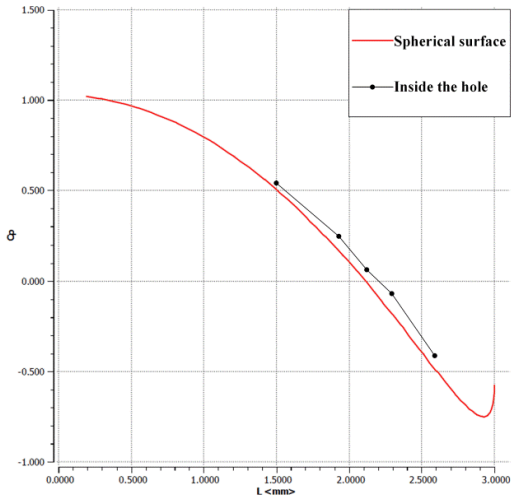

FIGURE 9. Pressure coefficient contrast curve of in-hole and surface.

three tests, and additional experiments are needed. The results of the additional experiments are shown in Table 8. The average static pressure coefficient of each factor recalculated is shown in Fig. 8.

Figure 8 shows the effect of three levels of each factor on pressure coefficient C_p. The data point in the figure is the average pressure coefficient $\bar{y}_{jk}$ corresponding to three factors at different levels. Combined with the curve of Figure 8 and the data of Table 7 and Table 8, it can be concluded that the influence of velocity and hole diameter on pressure coefficient is small and negligible. When the hole diameter is 0.4 mm and 0.6 mm, the pressure coefficient is similar, which is less than 0.8 mm, so the hole diameter can be selected as 1/10 probe diameter. The hole angle has a significant effect on the pressure coefficient, when the hole angle is 45°, it is the optimal level. For the probe with perpendicular holes, the hole angle should be selected near 45°. Figure 9 shows the pressure coefficient contrast curve of the in the hole and the surface. The variation trend of the pressure coefficient in the hole is in good agreement with the surface pressure coefficient, which shows it can better reflect the surface pressure distribution of the probe.

VI. CONCLUSION

In this paper, taking the hemispherical 7-hole probe as the research object, the influence of probe structure parameters on the measurement of pressure coefficient at different speeds is analyzed. The orthogonal experimental design method was used to design the experimental scheme of three levels and three factors, and the additional experiments were carried out according to the experimental results, which reduced the number of experiments to the greatest extent. The numerical simulation was carried out by Fluent software, and the pressure coefficient values of the hemispherical seven-hole probe under various structural parameters were calculated. The range analysis of the results was carried out, and the influence of various structural parameters on the pressure coefficient measurement was obtained. The numerical simulation results show that the perpendicular holes are better than the forward-facing holes. The velocity and hole diameter have little influence on the pressure coefficient measurement, and the hole angle is the most significant factor affecting the pressure coefficient measurement. It is determined that the optimal angle range of the hemispherical 7-hole probe with perpendicular holes is about 45°, and the hole diameter is 1 / 10 of the probe diameter, which provides reference for the optimization design of the hemispherical 7-hole probe. This study only optimized the structure of the hemispherical 7-hole probe; however, the concept of an optimal hole position can also be applied to other probes. However, this study only discusses the subsonic situation, and whether the speed has an effect at high speed needs to be further studied.

CONFLICT OF INTERESTS

The author declares that there is no conflict of interests regarding the publication of this paper.

ACKNOWLEDGMENT

The authors would like to thank Editage (www.editage.cn) for English language editing.

REFERENCES

[1] G. Wu, X. Guo, K. Yang, and H. Yang, "A robust calibration method for seven-hole pressure probes," *Exp. Fluids*, vol. 60, no. 8, pp. 1–16, Aug. 2019.

[2] A. L. Treaster and A. M. Yocum, "The calibration and application of five-hole probe," *Instrum. Soc. Amer. Trans.*, vol. 18, no. 3, pp. 23–34, 1979.

[3] A. J. Pisasale and N. A. Ahmed, "Theoretical calibration for highly three-dimensional low-speed flows of a five-hole probe," *Meas. Sci. Technol.*, vol. 13, no. 7, p. 1100, 2002.

[4] G. G. Zilliac, "Calibration of seven-hole probes for use in fluid flows with large angularity," Nat. Aeronaut. Space Admin., Ames Res. Center, Moffett Field, CA, USA, Tech. Rep. NASA TM 102200, 1989.

[5] P. V. Vukoslavčevič and D. V. Petrovič, *Multiple Hot-Wire Probe Measurements of Turbulent Velocity and Vorticity Vector Fields*, vol. 39, 21st ed. Podgorica, Montenegro: Montenegrin Academy of Sciences and Arts, Section of Natural Sciences, 2000.

[6] N. Sitaram and K. Srikanth, "Effect of chamfer angle on the calibration curves of five hole probes," *Int. J. Rotating Mach.*, vol. 2014, Jan. 2014, Art. no. 704315.
[7] H. Wang, X. Chen, and W. Zhao, "Development of a 17-hole omnidirectional pressure probe," *AIAA J.*, vol. 50, no. 6, pp. 1426–1430, 2015.
[8] B. F. Hall and T. Povey, "The Oxford probe: An open access five-hole probe for aerodynamic measurements," *Meas. Sci. Technol.*, vol. 28, no. 3, pp. 1–12, 2017.
[9] D. Telionis, Y. Yang, and O. Rediniotis, "Recent developments in multi-hole probe (MHP) technology," in *Proc. 20th Int. Congr. Mech. Eng.*, Gramado, Brazil, Nov. 2009, pp. 15–20.
[10] J. Crawford and A. M. Birk, "Influence of tip shape on Reynolds number sensitivity for a seven hole pressure probe," *J. Eng. Gas Turbines Power*, vol. 135, no. 9, Sep. 2013, Art. no. 091602.
[11] D. P. Georgiou and K. F. Milidonis, "Fabrication and calibration of a sub-miniature 5-hole probe with embedded pressure sensors for use in extremely confined and complex flow areas in turbomachinery research facilities," *Flow Meas. Instrum.*, vol. 39, pp. 54–63, Oct. 2014.
[12] R. G. Dominy and H. P. Hodson, "An investigation of factors influencing the calibration of five-hole probes for three-dimensional flow measurements," *J. Turbomach.*, vol. 115, no. 3, pp. 513–519, Jul. 1993.
[13] K. M. A. Díaz, J. M. F. Oro, E. B. Marigorta, and R. B. Perotti, "Head geometry effects on pneumatic three-hole pressure probes for wide angular range," *Flow Meas. Instrum.*, vol. 21, no. 3, pp. 330–339, Sep. 2010.
[14] T. Depolt and W. Koschel, "Investigation on optimizing the design process of multi-hole pressure probes for transonic flow with panel methods," in *Proc. Int. Congr. Instrum. Aerosp. Simulation Facilities (ICIASF)*. Rockville, MD, USA: IEEE Press, 1991, pp. 1–9.
[15] T. Depolt, F. Vinnemaier, and W. Koschel, "Investigation on minimizing blockage effects of multi-hole pressure probes in transonic flow," in *Proc. 10th Symp. Meas. Techn. Transonic Supersonic Flows Cascades Turbomach.* Brussels, Belgium: Von Karman Institute, 1990, pp. 17–18.
[16] V. V. Fedorov, *Theory of Optimal Experiments*. New York, NY, USA: Academic, 1972.
[17] J. H. Ferziger and M. Peric, *Computational Methods for Fluid Dynamics*. Berlin, Germany: Springer, 1999.
[18] K. N. Abed, Y. J. Almahdawi, and E. E. Kader, "Geometry modification effect on the aerodynamic characteristics of NACA 0015 using CFD," *IOP Conf. Ser., Mater. Sci. Eng.*, vol. 1076, no. 1, Feb. 2021, Art. no. 012067.
[19] R. Hassanzadeh, B. Sahin, and M. Ozgoren, "Numerical investigation of flow structures around a sphere," *Int. J. Comput. Fluid Dyn.*, vol. 25, no. 10, pp. 535–545, Dec. 2011.

TAO YAO received the B.S. degree in measurement and control technology and instruments from the Wuhan University of Technology, in 2016. He is currently pursuing the M.S. degree in instrument engineering with the National University of Defense Technology.

SHU-DAO ZHOU received the M.S. degree in system engineering from Southeast University, in 2000. He is currently a Professor with the National University of Defense Technology. His research interests include image processing, atmospheric detection, and electronic equipment design.

MIN WANG received the M.S. degree in control theory and control engineering from Hohai University, in 2008, and the Ph.D. degree in atmospheric science from the National University of Defense Technology, China, in 2019. She is currently an Associate Professor with the Nanjing University of Information Science and Technology.

SONG YE received the M.S. degree in signal and information processing from the PLA University of Science and Technology, in 2001, and the Ph.D. degree in navigation guidance and control from Southeast University, in 2005. He is currently an Associate Professor with the National University of Defense Technology, China.

YANG-CHUN ZHANG received the B.S. degree in electrical engineering and its automation from the North University of China, in 2019. He is currently pursuing the M.S. degree in atmospheric sciences with the National University of Defense Technology.